Journal of Nuclear Materials 390–391 (2009) 747–750

Contents lists available at ScienceDirect

Journal of Nuclear Materials

journal homepage: www.elsevier.com/locate/jnucmat

Arcing in ASDEX Upgrade with a tungsten first wall

A. Herrmann *, M. Balden, M. Laux, K. Krieger, H.W. Müller, R. Pugno, V. Rohde, ASDEX Upgrade team

Max-Planck-Institut für Plasmaphysik, Boltzmannstr. 2, D-85748 Garching, Greifswald, Germany

ARTICLE INFO

PACS:
52.40.H
52.55Fa

ABSTRACT

In-vessel inspections of AUG reveal arc tracks at different locations. This paper presents investigation of arcing at the inner transition and retention module where arc tracks were found around the whole toroidal circumference. A representative tile was investigated with profilometry, SEM, EDX, RBS, and colourimetry. Type 2 arc tracks with an area fraction of 12% were found in a 10 mm wide region near to the leading edge. Here the tungsten coating (3–4 μm) is removed and a small amount of carbon (max. 1–2 μm) is eroded. Droplets are detected at the surface. The region of the inner divertor where the arcs are observed shows a local enhancement of plasma density, $n_e \approx 10^{20}\,m^{-3}$, and neutral pressure, 0.1 mbar, favouring the arc ignition. A high sheath potential at the beginning of an ELM might trigger the arc. The arc pattern and the target load as measured with a fast IR-camera coincide. 2 g of tungsten are eroded in the inner divertor. If 10% of the material is eroded as droplets, 10^8 droplets (5 μm diameter) are ejected.

1. Introduction

In-vessel inspections performed routinely during the vessel venting of ASDEX Upgrade (AUG) reveal that arcs contribute significantly to the erosion of first wall materials. Two types of arc tracks are observed: a random walk of cathode spots due to unipolar arcs in non-magnetized glow discharges and arc tracks with a direction nearly perpendicular to the inclination of the local magnetic field from arcs burning during normal plasma operation. Usually, non-magnetized arc pattern are found on different in-vessel components: mirrors, shutters and diagnostic housings covered by thin layers from boronization and plasma operation. Here the arcs are removing the layers without damaging the base material seriously in consistency with the type 1 character of the cathode spots [1].

Cathode spots of arcs triggered during normal (magnetized) plasma operation are found at components that are in direct plasma contact such as the retention and transition module of the inner divertor but also at components remote from the plasma. Whereas the arc pattern in the divertor shows a toroidally symmetric distribution, arcs in remote areas are burning between components having a potential difference in the order of 100 V [2]. Technically, these arcs are suppressed by carefully checking distances of in-vessel components and the installation of shunt resistors limiting induced voltages. Whereas material released by arcs in remote areas has a low chance to penetrate into the scrape-off layer, Material released from the divertor region can contribute directly to the impurity content of the divertor plasma.

This paper is focused on the investigation of the regular arc pattern of the inner divertor with post mortem analysis techniques (Scanning Electron Microscopy (SEM), profilometry, colourimetry, Rutherford Back Scattering (RBS), and Energy-Dispersive X-ray spectroscopy (EDX)) as well as time resolved measurements of heat load, H_α radiation, and ion saturation currents.

2. Arcs during normal plasma operation in the inner divertor

The first campaign with ASDEX Upgrade as a full tungsten experiment started in 2007 with virgin tungsten coatings at the inner and outer strike zone and the transition module of the lower divertor. No boronization was performed during this campaign.

In-vessel inspection after about 500 plasma shots reveals that most of the tungsten coated target tiles in the lower divertor show no damages. Arc tracks are found at the transition and retention modules of the inner divertor, i.e. remote from the inner strike zone, the roof baffle and the upper passive stabilizing loop. Fig. 1 shows the transition and retention module of one section of AUG. For comparison, virgin tungsten coatings are shown at the right hand side of Fig. 1. It is obvious from Fig. 1 that a significant darkening can be observed at the right part of each target tile. This observation extends over the whole toroidal circumference with moderate variations due to the tile alignment with respect to the magnetic field. All 6 tiles of the transition module of one section were removed for further investigation. One representative tile was selected and characterized with respect to: the cathode spots (arc type, track density), the amount of eroded and deposited tungsten and carbon, as well as modifications of the surface. The results

* Corresponding author. Tel.: +49 89 32991388; fax: +49 89 3299 2580.
E-mail address: albrecht.herrmann@ipp.mpg.de (A. Herrmann).

0022-3115/$ - see front matter © 2009 Elsevier B.V. All rights reserved.
doi:10.1016/j.jnucmat.2009.01.296

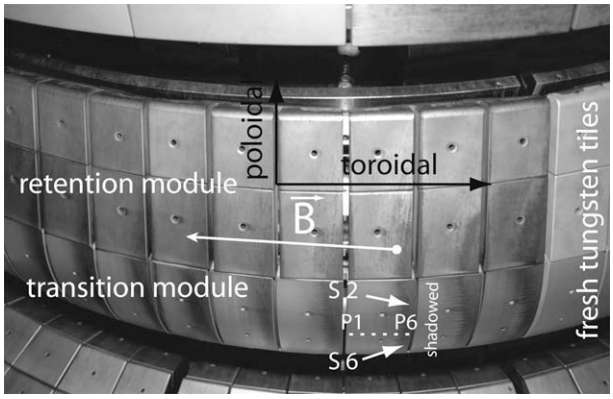

Fig. 1. Photo of the inner transition and retention module, showing the dark pattern at the right edge of each tile and the toroidal symmetry.

are presented and discussed in the following sub-section. In addition to the post mortem investigation fast cameras were installed to monitor the Hα radiation (Photron camera) and the heat load (IR-camera SBFP125) to the inner retention and transition module with a temporal resolution of about 100 μs/frame to characterize toroidal inhomogeneity of the arc pattern at a single target tile. The spatial resolution was 2 and 3 mm, respectively.

2.1. Results from post mortem characterization

One tile (5/2,Se1) was selected for post mortem analysis with a 3D optical profilometer (NanoFocus AF 2000, $\Delta z = 0.02$ μm, $\Delta x, \Delta y = 1$ μm), a FEG-SEM combined with a focused ion beam (FIB) for cross-sectioning (HELIOS Nanolab 600, FEI), a SEM with EDX for element sensitive measurements (XL30, FEI, with Genisis, EDAX), RBS to measure the spatial integrated amount of carbon and tungsten, as well as colourimetry to deduce the thickness of a carbon layer from the interference pattern [3].

Regions of about 10×20 mm^2 were sampled with the profilometer in the dark region (S2, S6 in Fig. 1) and averaged track parameters were derived along toroidal lines starting at the right edge of the scan region (Fig. 2). S2 represents an arcing region with a maximum toroidal extent near to the retention module, whereas S6 is located near to the strike point module were no arcing was found. The track width as well as the effective depth decrease with increasing distance from the edge of the tile. A decreasing width points to a decreasing total arc current because the current density is constant for a given material, i.e. the burning conditions become worse. The large width (150 μm) at the tile edge is partly due to an overlap of arc tracks. The crater depth is in average 5.5 μm at the edge of the tile. Having in mind that the thickness of the virgin tungsten layer is between 3.2 and 3.8 μm [4], this implies that carbon with a thickness of about 1–2 μm is eroded from the bottom of the arc tracks. About ten millimetres away from the tile edge (S2), the averaged crater depth is below the tungsten thickness because a part of the material eroded at the edge of the tile is redeposited in that region. A broad distribution of the arc track length between 0.5 and 3 mm with a pronounced maximum at 1,5 mm was derived from 31 identified arc tracks. Taking averaged spot velocities of 290 m/s as measured at 1 μm thick tungsten coatings [5] and that measured at massive tungsten (40 m/s for 10 A), the life time of an arc is in the range of 5–37 μs. The arc track density as derived from a scan region of 11×12 mm^2 at the dark edge is 12%.

SEM measurements allow a very detailed investigation of the surface. Moreover, the FIB is used for cross-sections at selected positions. This gives insight into the thickness of layers and deposits as well as in the re-crystallization process of tungsten due to the temperature excursions caused by an arc. A typical example is shown in Fig. 3, right. The picture is taken from a region of S6 (see Fig. 1). It shows a high track density with a significant fraction of very short tracks (spots). This spots are probably due to arcs that ignite but could not burn. FIB which was tilted 52° to the surface normal was used for depth profiling at selected positions. 3 horizontal cuts can be seen in Fig. 3. The measured thickness of the tungsten layer is about 4 μm, the thickness of the deposited layer up to 2 μm. Some arc tracks are buried by deposits. Most of the investigated craters have a flat bottom without significant carbon erosion.

A significant fraction of the tungsten is not evaporated by the arc but splashed of as liquid metal and redeposited as droplet. Such droplets are detected by SEM and profilometry not only in the crater bottom (see Fig. 3) but also at other surface areas. The consistency of such droplets and its role for dust generation is discussed in [6].

The EDX analysis of the surface (W-M line, C-K line) reveals that except for the rim of the crater there is no enhancement of tungsten around arc tracks. The deposited layer is a mixture of tungsten and carbon. Such layers are also found at the bottom of older tracks. Nearly pure tungsten is detected at the rim of fresh tracks. In turn, for those tracks the crater bottom is dominated by carbon.

This is supported by spatially (1×1 mm^2) integrated RBS measurements at six toroidal positions as indicated in Fig. 1 (P1-P6). A clean tungsten surface was found at position 1–4. The carbon coverage increases from 0.8 μm at position 5 to 1.8 μm at position 6 in the dark region of the target. The RBS values are moderately higher than the layer thickness taken from the micro beam cuts because for small angles of incidence carbon is buried in groves of the fresh coating and smoothing the surface (see Fig. 2 in [7]).

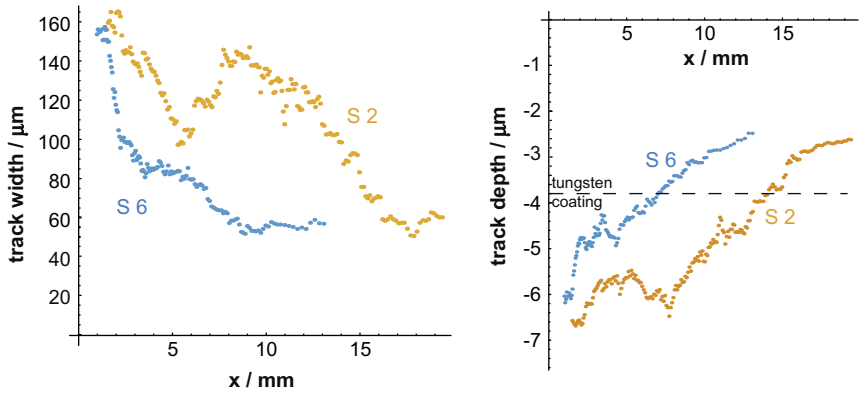

Fig. 2. Width (left) and depth (right) of arc tracks versus toroidal distance from the dark tile edge at sample position S2 and S6 (see Fig. 1).

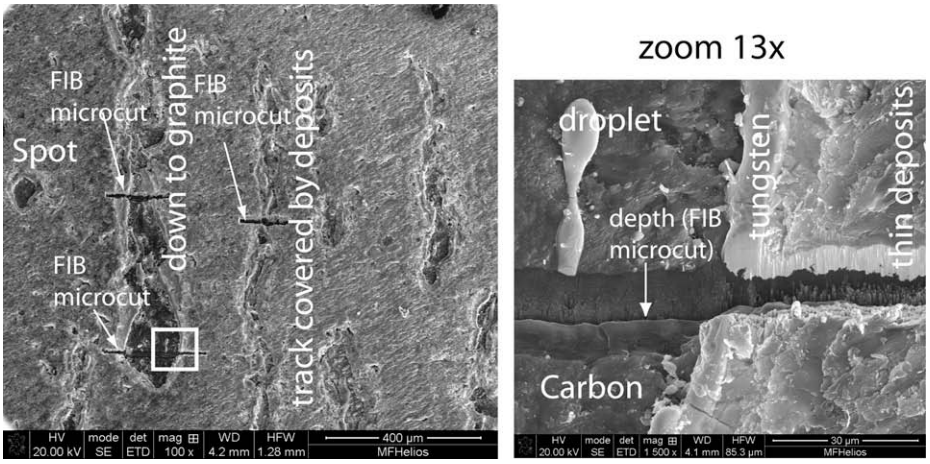

Fig. 3. SEM pictures of a sub-region of S 6 in Fig. 1 showing essential features as mentioned in Section 2.1. and FIB cross-section showing that there is nearly no erosion of carbon at the bottom of the arc track.

Table 1
Erosion due to arcs and the volume of the deposited layer for a single tile and extrapolated to the whole inner divertor. The transition and the retention tiles are considered with 24 cm poloidal height. The toroidal width of the arcing zone at a single tile is 11 mm.

	Single tile	Inner divertor
	mm^3 (mg)	
W erosion	0.7 (13.3)	100 (2 g)
C erosion	0.17 (0.35)	25 (50)
Deposition	2.5	360

Colourimetry could be applied only to one region in the lower part of the tile (below Sample 6) because it was difficult to find a continuous interference pattern. Here, the carbon deposition is about 0.4 μm at the outermost edge of the tile.

From the profilometer data and the SEM–FIB data, the amount of eroded and deposited material can be calculated (Table 1). The two grams of tungsten (3.2×10^{22} W-atoms/m^{-2}) eroded from the inner divertor by arcing are small compared to the erosion due to sputtering in the outer divertor and the outboard limiter as measured by spectroscopy [8]. But, if only 10% of the material is ejected as droplets of 5 μm in diameter, the number of droplets is 1.5×10^8.

2.2. In-situ measurements

The measurements in the visible and the IR-wavelength region are used to identify the toroidal asymmetry in density (H_α-radiation) in front of the target and the heat load. The IR-photon flux from the inner divertor tiles coincides well with the dark pattern from a photograph as shown in Fig. 4. The tiles of the transition

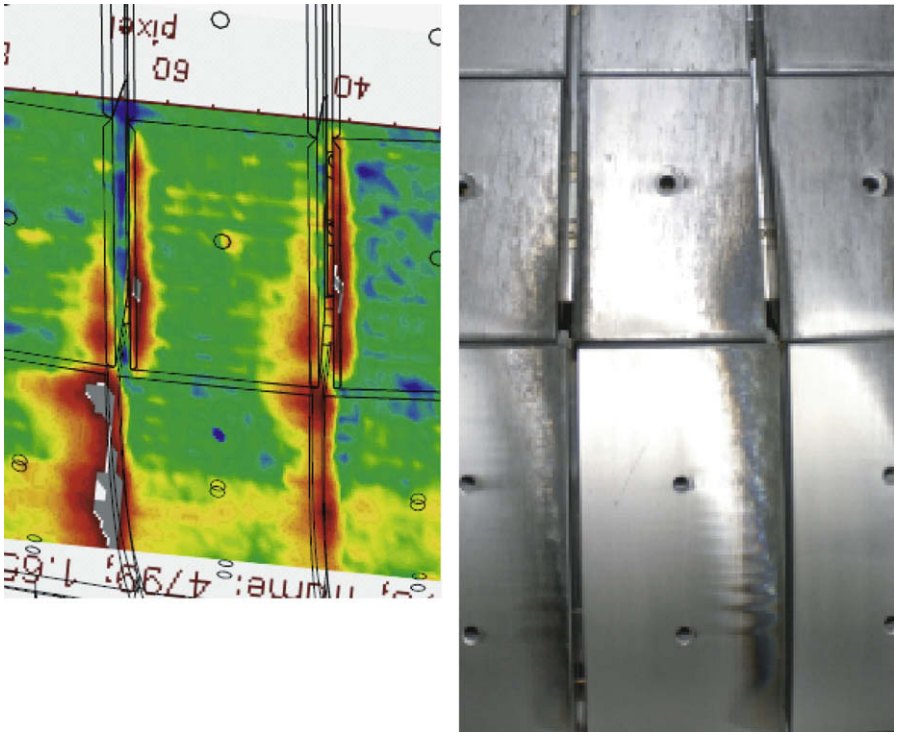

Fig. 4. View of the IR-camera and photo of an arc pattern of a comparable region in the inner divertor.

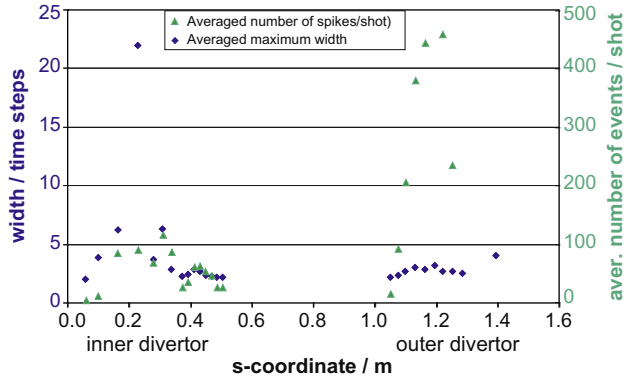

Fig. 5. Arc/filament statistic for all shots of the 2007 campaign. Calculated is the number of spikes in the Isat signal of Langmuir probes in the lower divertor resulting in a current limitation of the power supply and the temporal width (25 μs/time step) of the spikes. Plotted is average over all shots. The *s*-coordinate is the distance across the divertor surface.

module are tilted by 0.5° to shadow each other. No type 2 arc traces were found in the shadowed region. For the tiles of the retention module, which are not tilted, heat is loaded also to the unshadowed edge at the right hand side of the gap. Here, arc tracks are identified. The measured H_α-radiation is also higher in this region with high heat load and in the gaps between tiles.

There are only very few data for arc ignition in a strong magnetic field. It was shown in [9] that the voltage necessary to trigger an arc is lower for a given pressure at the low pressure side of the Paschen-curve, i.e. the conditions for arc triggering are improved in the presence of the magnetic field. Recent measurements [10] have shown that the transition and retention module of the inner divertor is a region with enhanced electron- and neutral density. Here values of up to $n_e = 2.5\times10^{20}\,m^{-3}$ and $n_0 = 1.5\times10^{21}\,m^{-3}$ are found, i.e. the neutral pressure is in the order of 0.1 mbar. The voltage required to ignite and drive an arc arises in the start phase of an ELM where the fast electrons increase the sheath potential in front of the target on a microsecond time scale.

Langmuir probes in the lower divertor are used to validate the appearance of arcs during plasma operation. The I_{sat} signals of all Langmuir probes in the lower divertor were analyzed according to the number of events resulting in a current limitation of the power supply. When such an event was found, the width was measured as shown in Fig. 5. The number of events is a factor of 5 higher in the outer divertor and is about the number of ELMs/shot. A single event lasts in average one time step (25 μs). In contrast, the typical width of an event (arc) is more than a factor of two higher for the retention and transition module in the inner divertor were the arc tracks are dominant.

3. Summary

In-vessel inspections of AUG reveal arc tracks at different locations, at tiles in direct plasma wall contact, such as divertor targets, as well as components remote from the plasma. The track orientation and pattern allow to distinguish between arcs burning during glow discharges and during normal magnetized plasma operation. This paper presents investigation of the arc dominated region in the lower divertor - the inner transition and retention module, where arc tracks were found around the whole toroidal circumference. A representative tile was investigated with profilometry, SEM, EDX, RBS, and colourimetry. Type 2 arc tracks covering 12% of the area were found in a 10 mm wide region near to the leading edge. Here the tungsten coating (3–4 μm) is removed and a small amount of carbon (max. 1–2 μm) is eroded from the bottom of the track resulting in a thin (max. 2 μm) deposited layer consisting of tungsten and carbon. Additionally, droplets splashed from the arc track are detected at the surface. The data for erosion and deposition are summarized in Table 1.

The region of the inner divertor where the arcs are observed shows a local enhancement for plasma density, $n_e \approx 10^{20}\,m^{-3}$, and neutral pressure, 0.1 mbar, favouring the arc ignition. A high sheath potential at the beginning of an ELM might trigger the arc. The arc pattern and the target load as measured with a fast IR-camera coincides, leading to the conclusion that the arcs get their energy from the flux tubes having a typical length of 10 m.

References

[1] B. Jüttner, V.F. Puchkarev, E. Hantzsche, et al., in: R.L. Boxman, P.J. Martin, D.M. Sanders (Eds.), Handbook of Vacuum Arc Science and Technology, Noyes, Park Ridge, NJ, 1995, p. 73 (Chapter 3).
[2] M. Laux, H. W. Müller, Experience from Langmuir Probe Voltage Variation at JET and AUG.
[3] P. Wienhold, F. Weschenfelder, J. Winter, Nucl. Instrum. Meth. Phys. Res., Sect. B 94 (1994) 503.
[4] S.E. Plansee, W-PVD Beschichtung von Feinkorngraphitziegeln - ASDEX Upgrade Hitzeschild, 2006.
[5] M. Laux, W. Schneider, B. Jüttner, et al., IEEE Trans. Plasma Sci. 33 (2005) 1470.
[6] M. Balden et al., these Proceedings, 2008.
[7] A. Herrmann, M. Balden, W. Bohmeyer, et al., Phys. Scrip. T 111 (2004) 98.
[8] R. Dux et al., J. Nucl. Mater. 390–391 (2009) 858.
[9] J. Rossignol, B. Jüttner, C. H. Wu, in: Twentieth Symposium on Discharges and Electrical Insulation in Vacuum – Tours, 2002.
[10] K. McCormick et al., J. Nucl. Mater. 390–391 (2009) 465.